Advances in Military Technology
Vol. 17, No. 1, 2022, pp. 33-45
ISSN 1802-2308, eISSN 2533-4123
DOI 10.3849/aimt.01542

Influence of Spike-Nosed Length on Aerodynamic Drag of a Wing-Projectile Model

V. Minh Do[1], T. Hung Tran[2*], X. Son Bui[1], D. Anh Le[3]

[1] *Faculty of Special Equipments, Le Quy Don Technical University, Hanoi, Vietnam*
[2] *Faculty of Aerospace Engineering, Le Quy Don Technical University, Hanoi, Vietnam*
[3] *School of Aerospace Engineering, VNU-University of Engineering and Technology, Hanoi, Vietnam*

The manuscript was received on 28 October 2021 and was accepted after revision for publication as research paper on 4 April 2022.

Abstract:

In this study, the effect of spike-nosed length on aerodynamic drag of a wing-projectile model was investigated at supersonic conditions. The projectile BK-13 with convex nose was selected for the study. The ratio of nose diameter and model diameter was fixed at around 0.34 while the ratio of the length of the nose and the model diameter was changed from 1.25 to 2.75. Numerical simulation with turbulent model k-ε was applied for flow structure around the model. The effect of mesh size and numerical models on the drag of the standard model was investigated. The study showed that numerical methods allow to obtain highly accurate drag coefficients. As the length of aerospike increases, the drag coefficient quickly decreases and obtains a minimum value at l/D = 2.0. The effect of spike-nosed length and velocity on flow pattern and drag of the model was explained in details in this study.

Keywords:

aerospike, drag coefficient, flow fields, numerical methods

1 Introduction

Reducing drag and increasing the aerodynamic performance of the flying object have been important topics for mechanic researchers for many years. To reduce the drag, a model was often designed with a streamline body. Consequently, the flow separation on the surface is delayed. The streamline body allows reducing the pressure drag which is acting on the model. However, since the capacity is required for moving objects, the streamline design is not always satisfied.

[*] *Corresponding author: Department of Aerospace Engineering, Le Quy Don Technical University, 236 Hoang Quoc Viet, Cau Giay, Hanoi, Vietnam. Phone +84 355 54 47 45, E-mail: tranthehung_k24@lqdtu.edu.vn*

Many blunted nose flying objects were designed with an aerospike. In fact, the aerospike is added to the nose and allows to move the conical shock wave far from the nose of the model. Consequently, the pressure around the nose decreases and the aerodynamic drag of the model decreases. The application of spike also allows to increase stability and to decrease heat transfer of the model [1]. However, the level of drag reduction depends on the geometry of the nose, and parameters of the spike, such as its length, diameter and nose configuration.

Previously, the effects of spike on flow structure around the nose and drag reduction were studied widely by both experimental and numerical approaches [2-9]. Stalder and Nielsen [1], who conducted measurements with spikes at high Mach number, indicated that aerodynamic drag of the model decreases with increasing length up to two times of diameter. Similar results were obtained by Ahmed and Qin [4], who applied a numerical simulation for studying the effect of aerospike on flow structure and drag of the model. Additionally, by adding an aero-disk to the spike nose, the drag of the model remarkably decreases. The application of the aero-disk allows to push the separation away from the spike and to reduce the pressure around the nose of the model. Kalimuthu et al. [10], who studied the effect of the spike-nosed length and its angle of attack on aerodynamic characteristics by experimental methods, showed that the static stability of the model increases with an added aerospike. The ability of aerospike and its mechanisms to reduce aerodynamic drag and to increase stability was then confirmed.

Although many studies have been conducted on the aerospike focused on drag reduction, previous studies mainly focused on hypersonic flow, where Mach is higher than 6. Additionally, the front part of the models in previous studies was often designed with convex curvature, such as sphere or ellipsoidal shape. The effect of aerospike on drag trend is not clear for specific models where the junctions between the model and aerospike are designed by a plate or a concave curvature shape, such as projectiles BK-13 of Russia and M431 of America. Moreover, although applications have been applied added to those models, the related data is not available. The detailed flow fields were not analyzed. Hence, to study the effect of aerospike on flow structure and drag reduction at supersonic flow is very important for further investigation. The study also helps to better understand and improve the design of the models which are currently used.

Nowadays, the development of technology provides a highly advantageous tool for analyzing fluid flow. In many cases, Navier-Stokes equations are solved by the finite volume method. The discrete results are then used to reconstruct the flow structure around the models. Reynolds-averaged Navier-Stokes (RANS) equations, Large Eddy Simulation (LES) and Direct Numerical Simulation (DNS) are the well-known technique for research. Although the current RANS method provides averaged flow fields, the low size of mesh requirement allows saving numerical time. The methods, consequently, are still widely applied in many recent studies [2, 3, 11-14]. The numerical studies also allow to extend results from experimental methods, which are often limited by measurement devices [15-17].

The present study investigates the effect of spike-nosed length on aerodynamic drag of a wing-projectile model at velocities from subsonic to supersonic conditions. A specific model which has a concave curvature junction was applied. The length of aerospike was changed to find the nose model with minimum drag. Flow behavior around the projectile was conducted by numerical approach with RANS methods. Turbulence model k-ε was applied for highly accurate results. The relation between

flow fields and drag will be presented in details. We have illustrated that there is an optimal spike-nosed length for minimum drag of the model at supersonic conditions. Additionally, the mechanism of aerospike at supersonic and hypersonic conditions in previous studies are very similar.

2 Numerical Methods

2.1 Model Geometry and Mathematical Models

The model which was used in this study is projectile BK-13 as shown in Fig. 1. This is a fin-stabilized, gun-fired explosive projectile and it is used against armored targets. At the junction part, six fins were added to reduce the reversed flow at the front part. The diameter D of the model equals 122 mm and its total length L is 631 mm. The ratio of the length to diameter is L/D = 5.17. The projectile uses an aerospike for reducing aerodynamic drag. For the baseline model, the diameter d of the aerospike is 42 mm and its length l is 213 mm. The ratio of the spike-nosed length to the diameter of the model was l/D = 1.75 while the ratio of the aerospike diameter to the model diameter was d/D = 0.34, which is similar to the ratio of the nose of the aerospike to the model diameter in the previous study by Ahmed and Qin [4]. Note that the diameter of the nose cannot be changed due to the structure and tactical requirements. In this study, we will change the length of the aerospike from l =1.25D to l =2.75D to investigate the effect of the length on the drag of the model. Note that the nose of the model was designed with the concave curvature shape, which is totally different from the previous studies studying the aerospike. Although the advantage of the spike on the drag reduction of that model has been presented, it is interesting to know the details of the flow phenomenon at high range of velocity. The total of seven models were applied to obtain the drag trend of the model. The free-stream Mach number was changed from 0.5 to 2.5 to study the effect of velocity on the drag of the model. The other parts of the models were maintained as original ones for validations of the numerical scheme. The initial numerical simulation indicated that the drag due to stability wings reaches to 57 % of the total drag of the model at Mach number of M = 2.0.

Fig. 1 Projectile model

The numerical domain has a size of 28D × 5D × 5D. In this study, we used sufficiently wide numerical domain to obtain the whole wake structure flow. Since the model geometry is complicated and this study focused on the averaged characteristics of the flow, the mesh in numerical domain was generated automatically. However, the

size of the mesh was changed depending on the distance from the model. In details, the size of the mesh around the model is significantly small with ten small uniform layers to obtain the correct boundary layer. The size of the mesh increases with the distance from the wall surface. Fig. 2 presents the mesh around the model surface for the original spike-nosed length.

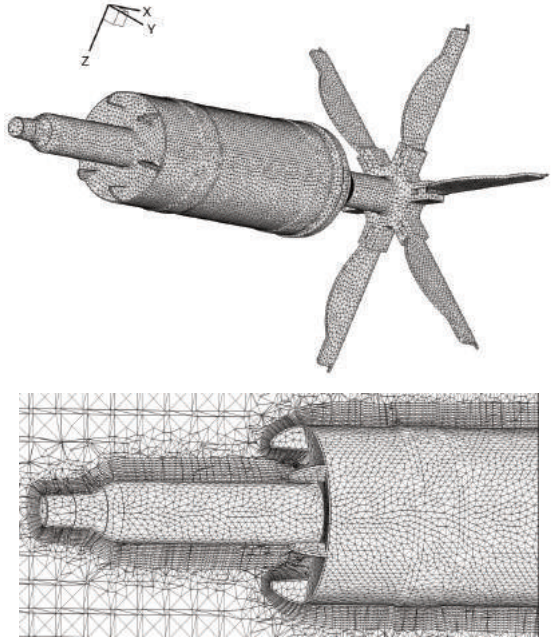

Fig. 2 Mesh around the model

2.2 Mathematical Model

This study used Reynolds averaged Navier-Stokes (RANS) equations for calculating the drag and analyzing the flow fields around the model. In RANS methods, an averaged filter was applied to Navier-Stokes equations. The Reynolds stresses are simulated by turbulent models. Although RANS method allows only averaged flow fields, it is efficient in reducing the numerical time and maintains sufficiently high accuracy. Navier-Stokes equations are shown as.

$$\frac{\partial p}{\partial t}+\frac{\partial(\rho u)}{\partial x}+\frac{(\rho v)}{\partial y}+\frac{(\rho w)}{\partial z}=0 \tag{1}$$

$$\frac{\partial(\rho u)}{\partial t}+\frac{\partial\left(\rho u^2\right)}{\partial x}+\frac{\partial(\rho uv)}{\partial y}+\frac{\partial(\rho uw)}{\partial z}=-\frac{\partial p}{\partial x}+\frac{1}{Re}\left(\frac{\partial \tau_{xx}}{\partial x}+\frac{\partial \tau_{xy}}{\partial y}+\frac{\partial \tau_{xz}}{\partial z}\right) \tag{2}$$

$$\frac{\partial(\rho v)}{\partial t}+\frac{\partial(\rho uv)}{\partial x}+\frac{\partial\left(\rho v^2\right)}{\partial y}+\frac{\partial(\rho vw)}{\partial z}=-\frac{\partial p}{\partial y}+\frac{1}{Re}\left(\frac{\partial \tau_{xy}}{\partial x}+\frac{\partial \tau_{yy}}{\partial y}+\frac{\partial \tau_{yz}}{\partial z}\right) \tag{3}$$

$$\frac{\partial(\rho w)}{\partial t}+\frac{\partial(\rho uw)}{\partial x}+\frac{\partial(\rho vw)}{\partial y}+\frac{\partial(\rho w^2)}{\partial z}=-\frac{\partial p}{\partial z}+\frac{1}{Re}\left(\frac{\partial \tau_{xz}}{\partial x}+\frac{\partial \tau_{yz}}{\partial y}+\frac{\partial \tau_{zz}}{\partial z}\right) \tag{4}$$

$$\begin{aligned}&\frac{\partial(E_T)}{\partial t}+\frac{\partial(uE_T)}{\partial x}+\frac{\partial(vE_T)}{\partial y}+\frac{\partial(wE_T)}{\partial z}=-\frac{\partial(up)}{\partial x}-\frac{\partial(vp)}{\partial y}-\frac{\partial(wp)}{\partial z}+\\&+\frac{1}{Re}\left[\frac{\partial}{\partial x}\left(u\tau_{xx}+v\tau_{xy}+w\tau_{yz}\right)+\frac{\partial}{\partial y}\left(u\tau_{xy}+v\tau_{yy}+w\tau_{yz}\right)+\frac{\partial}{\partial z}\left(u\tau_{xz}+v\tau_{yz}+w\tau_{zz}\right)\right]-\\&-\frac{1}{Re}\frac{1}{Pr}\left(\frac{\partial q_x}{\partial x}+\frac{\partial q_y}{\partial y}+\frac{\partial q_z}{\partial z}\right)\end{aligned} \tag{5}$$

where u, v and w are the velocity in x, y and z direction, respectively; p is the pressure, t is the time, ρ is the air density, τ is the deviatoric stress tensor, E is the total energy, q is the heat flux, Re is Reynolds number and Pr is Prandtl number.

The first equation describes the law of conservation of mass, the next three equations represent the law of conservation of momentum, and the last equation describes the law of conservation of energy.

Turbulent model k-ε was selected for this study. The model was presented by Launder and Spalding [18], which allows to calculate turbulent eddy viscosity through kinetic energy k and dissipation rate ε. Although the model is insufficient for the flow near the wall, it captures well the flow fields around the model. The two additional equations for kinetic energy and dissipation rate are calculated as follows:

$$\begin{aligned}&\frac{\partial(\rho k)}{\partial t}+u\frac{\partial(\rho k)}{\partial x}+v\frac{\partial(\rho k)}{\partial y}+w\frac{\partial(\rho k)}{\partial z}=\frac{\partial}{\partial x}\left[\left(\mu+\frac{\mu_t}{\sigma_k}\right)\frac{\partial k}{\partial x}\right]+\\&\frac{\partial}{\partial y}\left[\left(\mu+\frac{\mu_t}{\sigma_k}\right)\frac{\partial k}{\partial y}\right]+\frac{\partial}{\partial z}\left[\left(\mu+\frac{\mu_t}{\sigma_k}\right)\frac{\partial k}{\partial z}\right]+P_k-\rho\varepsilon\end{aligned} \tag{6}$$

$$\begin{aligned}&\frac{\partial(\rho\varepsilon)}{\partial t}+u\frac{\partial(\rho\varepsilon)}{\partial x}+v\frac{\partial(\rho\varepsilon)}{\partial y}+w\frac{\partial(\rho\varepsilon)}{\partial z}=\frac{\partial}{\partial x}\left[\left(\mu+\frac{\mu_t}{\sigma_k}\right)\frac{\partial \varepsilon}{\partial x}\right]+\\&\frac{\partial}{\partial y}\left[\left(\mu+\frac{\mu_t}{\sigma_k}\right)\frac{\partial \varepsilon}{\partial y}\right]+\frac{\partial}{\partial z}\left[\left(\mu+\frac{\mu_t}{\sigma_k}\right)\frac{\partial \varepsilon}{\partial z}\right]+C_{1\varepsilon}\frac{\varepsilon}{k}P_k-C_{2\varepsilon}\rho\frac{\varepsilon^2}{k}\end{aligned} \tag{7}$$

where function P_k is determined as

$$P_k=\tau_{xx}\frac{\partial u}{\partial x}+\tau_{xy}\frac{\partial u}{\partial y}+\tau_{xz}\frac{\partial u}{\partial z}+\tau_{yx}\frac{\partial v}{\partial x}+\tau_{yy}\frac{\partial v}{\partial y}+\tau_{yz}\frac{\partial v}{\partial z}+\tau_{zx}\frac{\partial w}{\partial x}+\tau_{zy}\frac{\partial w}{\partial y}+\tau_{zz}\frac{\partial w}{\partial z} \tag{8}$$

In Eqs (6) to (8), k is the kinetic energy, ε is the dissipation rate, E_{ij} represents the component of the rate of deformation, and μ_t represents the eddy viscosity. $C_{1\varepsilon}$, $C_{2\varepsilon}$, σ_k and σ_ε are constant numbers. They are determined as $C_{1\varepsilon}$ = 1.44, $C_{2\varepsilon}$ =1.92, σ_k =1.00 and σ_ε = 1.30.

The turbulent viscosity μ_t is shown by below equations:

$$\mu_t=\rho C_\mu\frac{k^2}{\varepsilon} \tag{9}$$

where C_μ = 0.0845 is constant numbers.

Navier-Stokes equations are solved by commercial software Ansys Fluent Version 12.1, which was copyrighted by the Faculty of Aerospace Engineering, Le Quy Don Technical University, Hanoi, Vietnam. RANS equations with turbulent models k-ε were selected for this study. The effect of the turbulent model on the results of the drag coefficients was presented in Section 2.4. The finite volume method with second order of numerical accuracy for pressure, density, momentum and turbulent kinetic energy was used for this study. The air is considered as ideal gas and viscosity was selected as Sutherland model. The SIMPLE algorithm was applied for the simulation. The residual convergence was set up at 10^{-5}.

2.3 Effect of Turbulent Models on the Drag of the Model

The selection of turbulent model is important for the accuracy of the results. In fact, the accuracy of C_D determination up to 1 % is required to calculate projectile trajectories. Since the mesh was generated automatically in this study, we checked the effect of different turbulent model in the numerical results. In details, the one equation turbulent model Spalart-Allmaras and two equation turbulent models k-ε and k-ω were applied for the standard model (l/D =1.75) at Mach number of 2.0. The size of the mesh was 3.6 million cells. Drag coefficients for different models were indicated in Fig. 3. Interestingly, the drag coefficient changes slightly for different turbulent models. Hence, the static results can be calculated and compared. The turbulent models k-ε were selected for accurate results and saving time. The same turbulent model was also used by Mansour and Khorsandi [2] for studying the drag reduction of aerospike model in hypersonic flow.

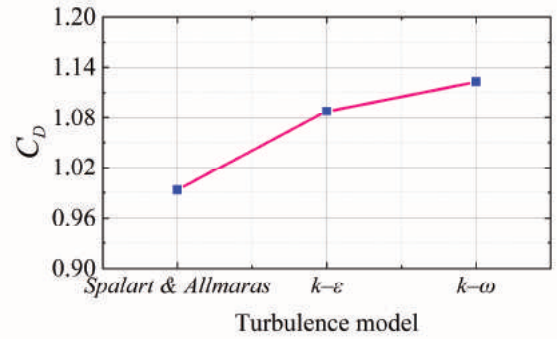

Fig. 3 Effect of selecting turbulent model on drag of the model

2.4 Mesh Independent Study

Since the mesh was generated automatically, different methods were applied to validate the numerical results. Firstly, mesh independence was studied. The volume of the mesh was changed in the range between 1.0 million cells to 3.6 million cells. We examined the drag coefficient for different mesh sizes at the velocity of V = 690 m/s. Numerical algorithm was the same as described in Section 2.2. Turbulent model k-ε was selected. Numerical results are indicated in Fig. 4. Clearly, the drag coefficient of the model is around C_D = 1.0 and it reduces slightly with increasing the mesh size. It indicates that the size of the mesh in the range from 1.0 million cells to 3.6 million cells does not strongly affect the drag of the model. Therefore, for 3D RANS simula-

tion, the mesh with the size of above 2 million cells could give sufficiently accurate results. Previously, Mansour and Khorsandi [2] indicated that the mesh with 2.8 million cell element provided close results to experimental data for study of the aerospike at Mach number of 6 and Reynolds number around 0.5×10^6. Zhong et al. [11] showed that the results calculated for aero-disk blunt body at Mach number of 6.8 were similar for mesh above 2.6 million cells. To obtain highly accurate results, the mesh with 3.6 million cells was selected for all test cases. The size of the mesh is higher than in the previous studies of spike at supersonic conditions.

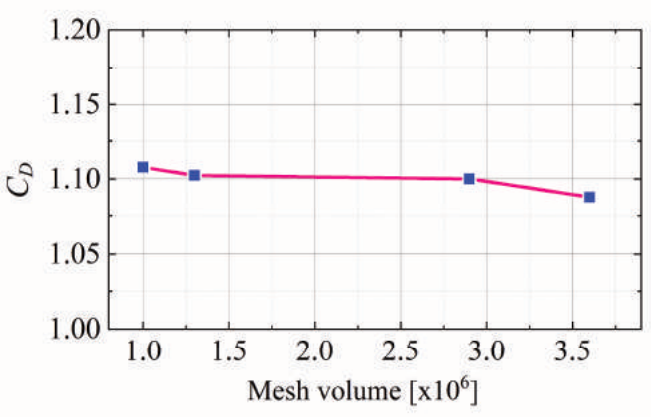

Fig. 4 Effect of mesh size on drag of the model

In this study, mesh independence studies were conducted. However, since the experimental force measurement for the model has not been published before, some limitations in validation exist. To achieve accurate results, experimental methods are required. Since this study focuses on the effect of the geometry on the drag trend, we did not conduct experiments.

3 Results and Discussions

3.1 Flow Fields around the Model

Fig. 5 shows the pressure fields around the original model (l/D = 1.75) on symmetric plane. The shock wave can be observed from the pattern of pressure. Clearly, a large shock wave is formed on the nose and convex flange around the model. However, the shock wave on the flange is quite small by comparison to the one around the nose. Clearly, the existence of the shock wave leads to the redistribution of the pressure on the surface, which often results in increasing the drag of the model. The large reversed flow around the base is a result in high drag. The details of the effect of the rear part on the drag will be analyzed in Section 3.5.

3.2 Effect of Spike-Nosed Length on Aerodynamic Drag

Fig. 6 shows the drag coefficient of the model for different lengths of the spike at the velocity of V = 690 m/s. Here, the reference area is the maximum cross-section area of the main body. Generally, drag of model quickly decreases with increasing the length of spike. The minimum drag is observed at around l/D = 2.0, where the drag reduces

by around 20 % in comparison to the case of *l/D* = 1.25. The drag slightly increases again at *l/D* above 2.0. The drag trend for different *l/D* was similar to the previous observation by Hutt and Howe [6] by experimental methods and Zhong et al. [11] by numerical approach. However, Mach number in the previous studies is much higher than in the current study. Clearly, the spike is not always effective in reducing the drag of model. Applying a long spike-nosed length can lead to an increase in the drag and the reduction of the structure stability of the model. Numerical results also indicate that the drag is mainly formed by pressure component. The drag due to the skin friction is around 2 % of the total drag. The change of the drag behavior is mainly generated by different structure of the shock wave and recirculation region on the nose of the model.

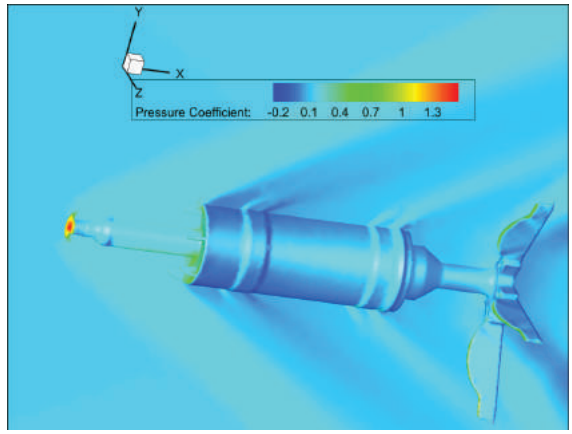

Fig. 5 Distribution pressure around the model

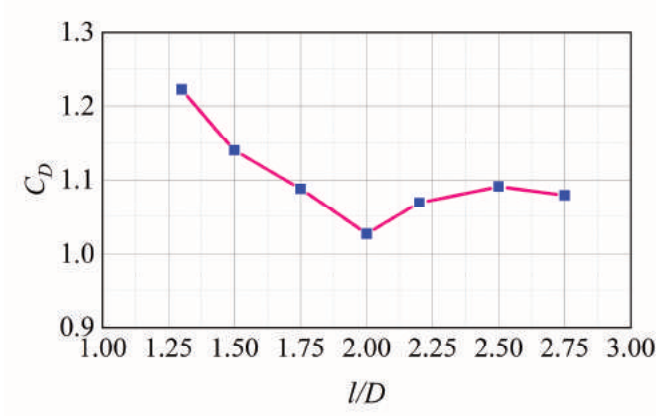

Fig. 6 Effect of spike-nosed length on drag of model

Note that the ratio of the length to the diameter with a minimum drag (*l/D* = 2.00) is different from the original model where *l/D* =1.75. It is probably because the drag is not the only parameter which should be considered in designing the model. In fact, the total model length, initial propulsion force, its stability and combat effectiveness are the other factors important in the designing process.

3.3 Flow around the Nose

Fig. 7 shows the streamlines around the nose of the model for different spike-nosed lengths. Analyzing the structure allows to explain the detailed drag trend of the model. Since the rear part is the same for different spike-nosed lengths, we assume that the difference in drag among those models depends on the length of the spike.

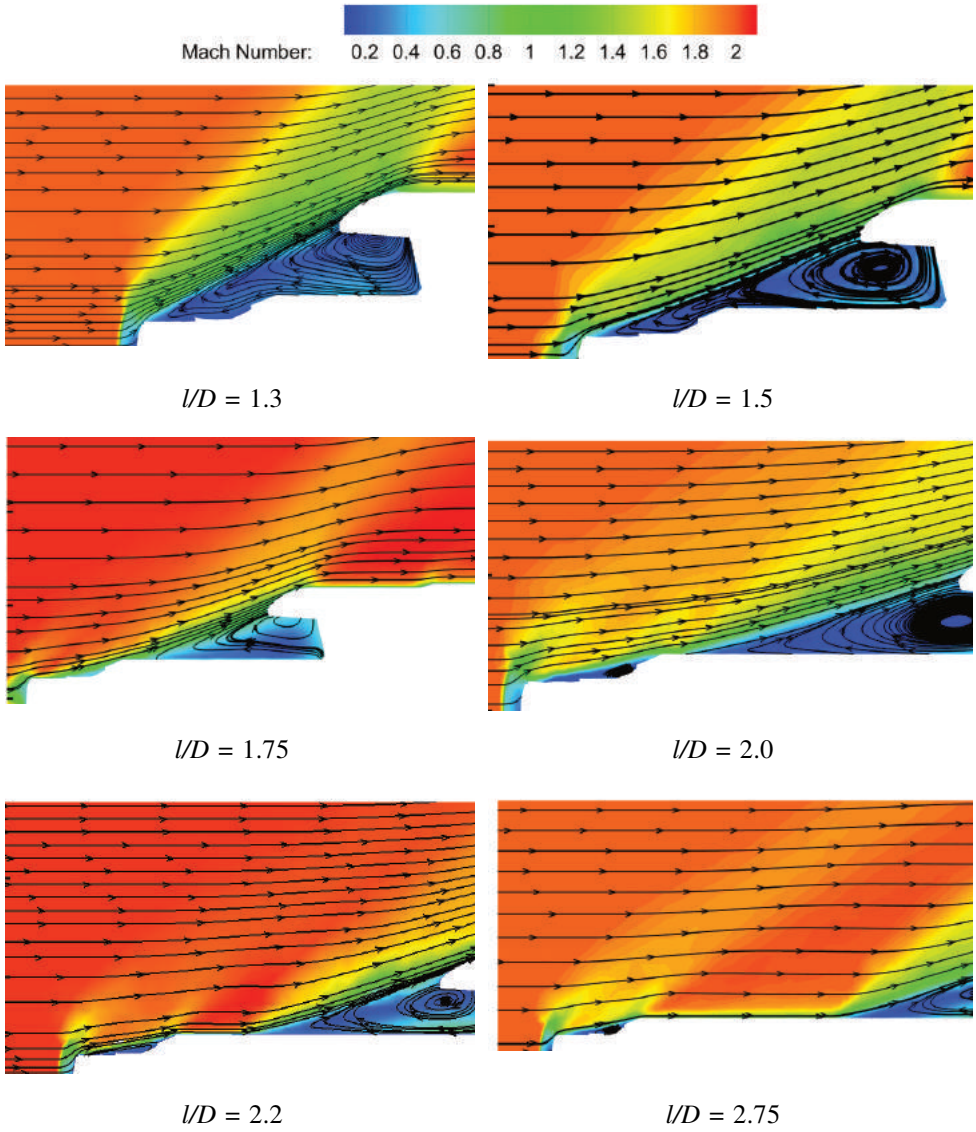

Fig. 7 Flow around the nose of model

Clearly, when the length is small, a recirculation region is formed and covers the whole nose. The structure of the flow is similar to the flow of an axisymmetric nose at supersonic flow. In that case, the drag of the model is sufficiently high. However, as

the length of spike increases, the reversed flow region on the model becomes narrow. As the results show, the drag of the model decreases. However, when the length is sufficiently high, two shock waves are formed around the nose. The effect of the shock wave leads to a slight increase in the drag of the model. Fig. 7 also indicated that the distribution of the velocity fields is very different for both short and long aerospike models.

3.4 Effect of Velocity on the Drag

Since the velocity of the projectile reduces in trajectory, it is significant to consider the drag of the model for different velocity flow conditions. The effect of the velocity on the drag of model was shown in Fig. 8. Although some uncertainty occurs for drag calculation around transonic flow, a clear trend of the drag is obtained for different spike-nosed length. Notably, the spike also has a positive effect on the drag reduction at low subsonic and transonic conditions, although the effect is not significant. At spike-nosed length of 1.3*D*, the drag is significantly high for all velocity cases. However, the drag reduces with increasing the spike-nosed length. It could be explained in such a way that the flow at a small spike-nosed length is characterized by a large reversed flow region, which results in high drag level.

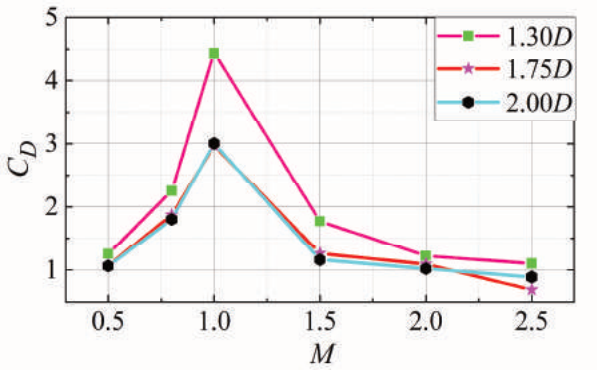

Fig. 8 Effect of flow velocity on drag

Fig. 9 shows the velocity fields around the model at subsonic, transonic and supersonic conditions for the original model (l/D = 1.75). For all cases, the flow around the model is featured by large separation regions around the noses and rear part of the model. The large wake flow was also noted well in the previous studies by Tran and Chen [19]. Tran et al. [20] also indicated that flow on the rear surface can affect the drag of the model. However, their study was conducted at low-speed conditions. In fact, a shock wave is formed at supersonic flow. The formation of shock wave reduces the boundary layer thickness and prevents separation on the main-body surface. For the case of subsonic flow, the separation flow occurs near the flanges, which increases the boundary layer thickness and the wake structure. Consequently, we observed a similar level of the drag at subsonic and supersonic conditions. The shock wave is formed on the nose of the model at transonic flow. However, the structure of the shock wave is quite different from the case of supersonic flow. It should be noted that the position of the shockwave at transonic and supersonic conditions are rather different. The large shock wave on the model and around the base leads to the high drag level at transonic conditions.

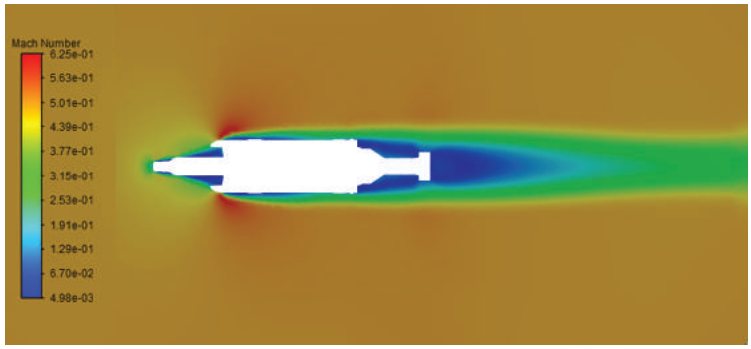

a. $M = 0.5$

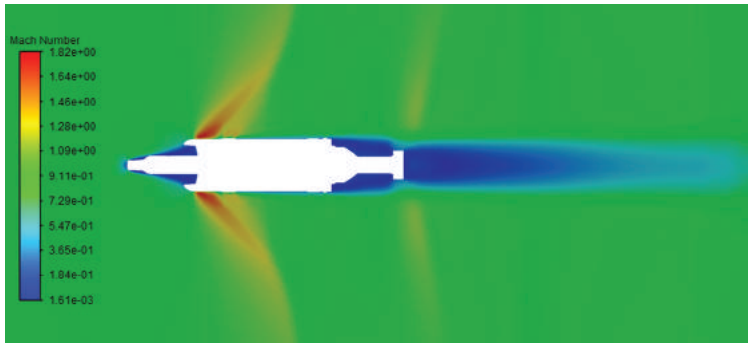

b. $M = 1.0$

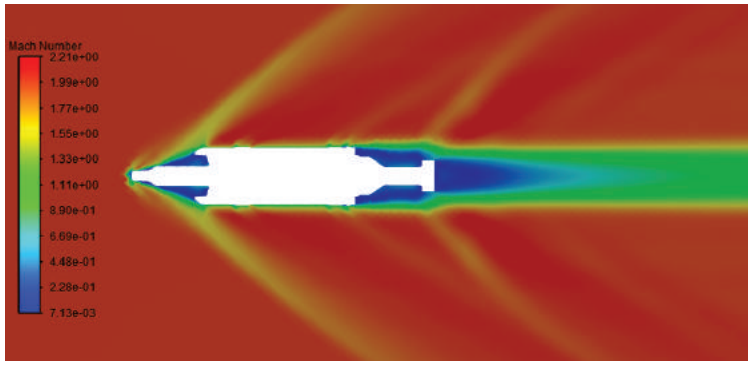

c. $M = 2.0$

Fig. 9 Flow around the model at different Mach number (l/D = 1.75)

4 Conclusions

The flow around the nose of a projectile using the aerospike for reducing the drag was studied by a numerical method. The comparisons of the drag coefficient for different sizes of the mesh and different numerical turbulent models were presented. The aero-

spike shows an effective method for reducing the drag of the model at supersonic flow. The main conclusion of this study is as follow:

The drag coefficient of the model quickly decreases with an increasing length of the spike up to $l/D = 2$. However, the increasing length of the spike above $2D$ leads to a slight increase in the drag again. The optimal spike-nosed length for a minimum drag is expected around $l/D = 2$ at the supersonic flow for the model with a diameter of $d/D = 0.34$. The use of spike also has a positive effect on the drag reduction at subsonic and transonic flow.

A large shock wave occurs around the nose of the model for different spike-nosed lengths. Recirculation flows are formed around the nose of the model. When the length of the spike is low, the recirculation covers the whole nose and drag of the model is sufficiently high. When the spike-nosed length is high, the recirculation region around the nose becomes small, which results in decreasing drag.

Finally, the results of this study can be used for further investigation and design of the projectiles with a similar geometrical structure.

References

[1] STALDER J.R. and H.V. NIELSEN. *Heat Transfer from a Hemisphere-Cylinder Equipped with Flow-Separation Spikes* [Technical note]. Washington: NACA, 1954.

[2] MANSOUR K. and M. KHORSANDI. The Drag Reduction in Spherical Spiked Blunt Body. *Acta Astronautica,* 2014, **99**(1), pp. 92-98. DOI 10.1016/j.actaastro.2014.02.009.

[3] NARAYAN A., S. NARAYANAN and R. KUMAR. Hypersonic Flow Past Nose Cones of different Geometries: a Comparative Study. *Simulation*, 2018, **94**(8), pp. 665-680. DOI 10.1177/0037549717733051.

[4] AHMED M.Y.M. and N. QIN. Drag Reduction Using Aerodisks for Hypersonic Hemispherical Bodies. *Journal of Spacecraft and Rockets*, 2010, **47**(1), pp. 62-80. DOI 10.2514/1.46655.

[5] DAS S., P. KUMAR and J.K. PRASAD. Hypersonic Flow over Hemispherical Blunt Body with Spikes. *Scientia Iranica*, 2019, **26**(1B), pp. 358-366. DOI 10.24200/sci.2018.20339.

[6] HUTT G.R. and A.J. HOWE. Forward Facing Spike Effects on Bodies of Different Cross Section in Supersonic Flow. *The Aeronautical Journal*, 1989, **93**(926), pp. 229-234. DOI 10.1017/S0001924000017085.

[7] HUANG W., Z. CHEN, L. YAN, B. BIN and D.Z. BO. Drag and Heat Flux Reduction Mechanism Induced by the Spike and its Combinations in Supersonic Flows: A Review. *Progress in Aerospace Science*, 2018, **105**(9), pp. 31-39. DOI 10.1016/j.paerosci.2018.12.001.

[8] Z. EGHLIMA and K. MANSOUR. Drag Reduction for the Combination of Spike and Counterflow Jet on Blunt Body at High Mach Number Flow. *Acta Astronautica,* 2016, **133**(11), pp. 103-110. DOI 10.1016/j.actaastro.2017.01.008.

[9] ANTONETS A.V. Application of the Method of Invariant Relations in Analyzing the Parametric Dependences of the Aerodynamic Parameters of the Classical Axisymmetric Noses of Flight Vehicles. *Fluid Dynamics*, 2015, **50**(2), pp. 272-282. DOI 10.1134/S0015462815020118.

[10] KALIMUTHU R., R.C. MEHTA and E. RATHAKRISHNAN. Experimental Investigation on Spiked Body in Hypersonic Flow. *The Aeronautical Journal*, 2008, **112**(1136), pp. 593-598. DOI 10.1017/S0001924000002554.

[11] ZHONG K., C. YAN, S.S. SHENG, T.Z. XIN and S. LOU. Aerodisk Effects on Drag Reduction for Hypersonic Blunt Body with an Ellipsoid Nose. *Aerospace Science and Technology*, 2019, **86**(6), pp. 599-612. DOI 10.1016/j.ast.2019.01.027.

[12] TRAN T.H., H.Q. DINH, H.Q. CHU, V.Q. DUONG, C. PHAM and V.M. DO. Effect of Boattail Angle on Near-wake Flow and Drag of Axisymmetric Models: a Numerical Approach. *Journal of Mechanical Science and Technology,* 2021, **35**(2), pp. 563-573. DOI 10.1007/s12206-021-0115-1.

[13] LE, D.A., T.H. PHAN and T.H. TRAN. Assessment of Homogeneous Model for Simulating a Cavitating Flow in Water Under a Wide Range of Temperatures. *ASME Journal of Fluids Engineering*, 2021, **143**(10), 101204. DOI 10.1115/1.4051078.

[14] LE, D.A. and T.H. TRAN. Improvement of Mass Transfer Rate Modeling for Prediction of Cavitating Flow. *Journal of Applied Fluid Mechanics*, 2022, ISSN 1735-3572 (in press).

[15] TRAN, T.H., T. AMBO, T. LEE, L. CHEN, T. NONOMURA and K. ASAI. Effect of Boattail Angles on the Flow Pattern on an Axisymmetric Afterbody Surface at Low Speed. *Experimental Thermal and Fluid Science*, 2018, **99**, pp. 324-335. DOI 10.1016/j.expthermflusci.2018.07.034.

[16] TRAN, T.H. and L. CHEN. Wall Shear Stress Extraction by an Optical Flow Algorithm with a Sub-grid Formulation. *Acta Mechanics Sinica*, 2021, **37**(1), pp 65-79. DOI 10.1007/s10409-020-00994-9.

[17] TRAN, T.H. The Effect of Boattail Angles on the Near-wake Structure of Axisymmetric Afterbody Models at Low-speed Condition. *International Journal of Aerospace Engineering*, 2020, 7580174. DOI 10.1155/2020/7580174.

[18] LAUNDER B.E. and D.B. SPALDING. The Numerical Computation of Turbulent Flows. *Computer Methods in Applied Mechanics and Engineering*, 1974, **3**(2), pp. 269-289. DOI 10.1016/0045-7825(74)90029-2.

[19] TRAN T.H. and L. CHEN. Optical-Flow Algorithm for Near-Wake Analysis of Axisymmetric Blunt-Based Body at Low-Speed Conditions. *Journal of Fluids Engineering*, 2020, **142**(11), pp. 1-10. DOI 10.1115/1.4048145.

[20] TRAN, T.H., T. AMBO, T. LEE, K. OZAWA, L. CHEN, T. NONOMURA and K. ASAI. Effect of Reynolds Number on Flow Behavior and Pressure Drag of Axisymmetric Conical Boattails in Low-Speed Conditions. Experiments in Fluids, 2019, **60**(3), pp. 1-19. DOI 10.1007/s00348-019-2680-y.